ELSEVIER

Nuclear Physics A 628 (1998) 41–61

NUCLEAR PHYSICS A

Study of odd-mass $N = 82$ isotones with realistic effective interactions

J. Suhonen [a,*], J. Toivanen [a], A. Holt [b], T. Engeland [b], E. Osnes [b], M. Hjorth-Jensen [c]

[a] *Department of Physics, University of Jyväskylä, P.O. Box 35, FIN-40351 Jyväskylä, Finland*
[b] *Department of Physics, University of Oslo, N-0316 Oslo, Norway*
[c] *Nordita, Blegdamsvej 17, DK-2100 København Ø, Denmark*

Received 8 September 1997; revised 1 October 1997; accepted 28 October 1997

Abstract

The microscopic quasiparticle-phonon model (MQPM) is used to study the energy spectra of the odd $Z = 53$–63, $N = 82$ isotones. The results are compared with experimental data, with the extreme quasiparticle-phonon limit and with the results of an unrestricted $2s1d0g_{7/2}0h_{11/2}$ shell model (SM) calculation. The interaction used in these calculations is a realistic two-body G-matrix interaction derived from modern meson-exchange potential models for the nucleon–nucleon interaction. For the shell model all the two-body matrix elements are renormalized by the $\hat{Q}$-box method, whereas for the MQPM the effective interaction is defined by the G-matrix.

PACS: 21.60.Jz; 21.60.Cs; 21.90.+f; 27.60.+j
Keywords: Spectra of odd $N = 82$ isotones; Microscopic quasiparticle-phonon model; Shell model; Realistic G-matrix-based effective interactions

1. Introduction

The quasiparticle-phonon coupling (QPM) scheme is a convenient way of exploiting the rich data on low-energy excitations of doubly-even nuclei in studying nuclear-structure effects in odd-mass (odd-A for short) nuclei. Since it was introduced [1] it has been used extensively, in various forms [2–8], to discuss energy spectra of odd-A nuclei. This scheme makes use of the property of the BCS quasiparticles being the

* Corresponding author.

PII S0375-9474(97)00615-5

elementary excitations of an odd-A nucleus and assumes that by coupling them to the few lowest-energy (collective) excitations of the doubly-even reference nucleus one is able to describe, at least qualitatively, the spectroscopy of odd-A nuclei. In many cases, only the first quadrupole and/or octupole phonon have been used in the calculations.

In the traditional quasiparticle-phonon models (QPM) independent model hamiltonians have been used to create the quasiparticles, the phonons and their coupling. This means that the two-body interaction matrix elements of the many-fermion hamiltonian are not internally consistent. For the phonons one usually adopts very simple model hamiltonians, like pairing-plus-quadrupole or semiempirical ones while the quasiparticle energies can be extracted from simple pairing hamiltonians or directly from experiments. The quasiparticle-phonon coupling term has usually the simplest possible phenomenological form and may have adjustable parameters to control the energy of the quasiparticle-phonon multiplets. In Ref. [8] a model was introduced, the so-called microscopic quasiparticle-phonon model (MQPM), which bears a resemblance to the traditional QPM, but which uses a microscopic hamiltonian and a scheme to optimize the size of the quasiparticle-phonon basis used in the calculations. In this sense (see the discussion in Section 2) it represents also an improvement over the traditional QPM since the quasiparticle-phonon interaction is treated in a more consistent way.

In order to test the MQPM method, we have singled out the $N = 82$ isotones. The sequence of semi-magic $N = 82$ nuclei shows a high degree of regularity which makes them well suited for systematic studies and for testing of microscopic nuclear models. Pairing effects seem to play an important role in the even nuclei, and the low-lying states in the odd nuclei may be described as one-quasiparticle states with increasing Fermi level. Thus, models like the MQPM may be viewed as a reasonable starting point for the description of such nuclei.

The first aim of this work is, therefore, to compare the MQPM with the more traditional QPM and QRPA approaches in order to see how well the experimental spectra can be reproduced and to interpret eventual differences.

A comprehensive study of the even $N = 82$ isotones was carried out by us in a previous work [9]. There, a comparison was made between the QRPA and the results obtained with an extensive shell model calculation. Energy spectra were generally well described and so were the transition probabilities. In Ref. [9] one of the aims was to calculate an effective interaction based on modern meson-exchange models for the nucleon–nucleon (NN) potential. The first step in the derivation of an effective interaction V_{eff} was to renormalize the NN potential through the so-called G-matrix. The G-matrix was in turn used in a perturbative many-body scheme (see, e.g., Ref. [10] for further details) to derive an effective interaction appropriate for the $N = 82$ isotones. The effective interaction is meant to take into account degrees of freedom not included in the model space. This interaction was, in turn, applied in a full shell model calculation with a model space consisting of the orbitals $2s_{1/2}$, $1d_{5/2}$, $1d_{3/2}$, $0g_{7/2}$ and $0h_{11/2}$ for the $Z = 52$–64, $N = 82$ isotones.

The second aim of this work is therefore to extend the comparative analysis of Ref. [9] for the even isotones to the case of the odd isotones. We will employ the same

effective interaction and model space in the shell model analysis. Moreover, the same G-matrix used in the QRPA studies of Ref. [9] will be used in the MQPM calculations. Since the MQPM discussed here (and the QRPA method of Ref. [9] as well) employs a larger single-particle space than the perturbative many-body scheme, our hope is to see whether the two approaches could shed light on different many-body contributions and their influence on various spectroscopic observables.

The $N = 82$ isotones have previously been studied extensively by Heyde and Waroquier [11,12] by using the quasiparticle Tamm–Dancoff approximation including one- and three-quasiparticle states as basis states and projecting out the spurious three-quasiparticle components. The calculations were performed using the surface-delta interaction [11] and a more elaborate phenomenological interaction [12] in the proton $2s_{1/2}1d_{5/2}1d_{3/2}0g_{7/2}0h_{11/2}$ single-particle basis, i.e. in the same basis which we adopt for the shell model in our present article. However, the more realistic results of Ref. [12] are not accessible for direct comparison with the present results of the MQPM for the following reasons. (i) The MQPM employs a larger valence space where neutron degrees of freedom are also included. (ii) In the MQPM we use the same proton single-particle energies, extracted from the experimental spectrum of ^{133}Sb, for all the odd isotones, whereas in Ref. [12] the inverse-gap-equation method was used to extract single-particle energies from the experimental spectra of each odd $N = 82$ isotone separately. (iii) In Ref. [12] the phenomenological force, namely a central force of Gaussian shape with spin exchange, was fitted from case to case by the above-mentioned inverse-gap-equation method, and overall by level schemes and transition rates of the even $N = 82$ isotones. Contrary to this, in the present MQPM calculation the same bare G-matrix interaction is used for all the even and odd $N = 82$ isotones without any fitting procedures. For the above reasons we refrain from direct comparison with the results of Ref. [12] in this article and, instead, make only a brief qualitative comparison with the results of Ref. [12] and almost exclusively concentrate on comparison with the shell model results.

The theoretical framework of the MQPM is presented in Section 2. A brief review of the effective interaction theory and the shell model follows in Section 3. The results are presented and discussed in Section 4. Finally, in Section 5 we draw our conclusions.

2. Theoretical framework of the MQPM

The microscopic quasiparticle-phonon model (MQPM) represents a scheme to treat all the three parts of the hamiltonian, namely the quasiparticle, phonon and quasiparticle-phonon terms, on equal footing. This is possible by starting from a microscopic hamiltonian with two-body matrix elements derived from effective matrix elements such as a G-matrix. The G-matrix is a medium modified nucleon–nucleon interaction where all ladder type diagrams are summed to infinite order. This method enables one in a systematic way to derive both the proton–neutron and the like-nucleon two-body interaction. In the quasiparticle language these parts of the interaction relate to the H_{31} and H_{22} parts of the quasiparticle representation of the nuclear hamiltonian. The H_{22} part is treated in the

BCS and quasiparticle random-phase approximation (QRPA) framework and leads to definition of the quasiparticles and the excitation (phonon) spectrum of the doubly-even reference nucleus. The H_{31} part is then diagonalized in the quasiparticle-phonon basis discussed below.

The MQPM treats the structure of the odd-A nuclei in four steps. First, the neighboring even–even nucleus, or nuclei, can be used to study the properties of the chosen mass region and to fix the possible free parameters of the model hamiltonian. In the present case, as also in Ref. [9], we have used a G-matrix derived from modern meson-exchange potential models, and thus no phenomenological renormalization of the two-body interaction was done. This hamiltonian is used to generate the phonons which are excitations of the even–even nuclei. In the MQPM the phonons are derived by the use of the quasiparticle random-phase approximation (QRPA) procedure [13]. Second, the monopole part of the same hamiltonian is used to generate the quasiparticles, which are the basic building blocks of the odd-A excitations, through the BCS procedure. As the third step, the two basic excitations, QRPA phonons and BCS quasiparticles, are coupled to form a wave function basis for a realistic treatment of the odd-A nucleus. As the last step, the residual hamiltonian, containing the interaction of the odd nucleon with the even–even reference nucleus (the $H_{31}+H_{13}$ part of the hamiltonian in Eq. (3) below), is diagonalized in this (over-complete) basis.

In the MQPM the starting point is the A-fermion hamiltonian

$$H = \sum_{\alpha} \varepsilon_{\alpha} c_{\alpha}^{\dagger} c_{\alpha} + \tfrac{1}{4} \textstyle\sum_{\alpha\beta\gamma\delta} \bar{v}_{\alpha\beta\gamma\delta} c_{\alpha}^{\dagger} c_{\beta}^{\dagger} c_{\delta} c_{\gamma}, \tag{1}$$

containing antisymmetrized two-body matrix elements $\bar{v}_{\alpha\beta\gamma\delta} = \langle \alpha\beta|v|\gamma\delta\rangle - \langle \alpha\beta|v|\delta\gamma\rangle$ obtained from the Bonn-A G-matrix. Greek indices denote all single-particle quantum numbers $\alpha = \{a, m_a\}$, and roman indices, when used, denote all single-particle quantum numbers except the magnetic ones, i.e. $a = \{n_a, l_a, j_a\}$.

The approximate ground state of the even–even reference nucleus is obtained from a BCS calculation, where quasiparticle energies and occupation factors u_a and v_a are obtained from the Bogoliubov–Valatin transformation to quasiparticles

$$\begin{aligned} a_{\mu}^{\dagger} &= u_{\mu} c_{\mu}^{\dagger} - v_{\mu} \tilde{c}_{\mu}, \\ \tilde{a}_{\mu}^{\dagger} &= u_{\mu} \tilde{c}_{\mu}^{\dagger} + v_{\mu} c_{\mu}, \end{aligned} \tag{2}$$

where $\tilde{a}_{\mu}^{\dagger} = a_{-\mu}^{\dagger}(-1)^{j+m}$ and $\tilde{c}_{\mu}^{\dagger} = c_{-\mu}^{\dagger}(-1)^{j+m}$. After this transformation the hamiltonian can be written in the form

$$H = \sum_{\alpha} E_a a_{\alpha}^{\dagger} a_{\alpha} + H_{22} + H_{40} + H_{04} + H_{31} + H_{13}, \tag{3}$$

where E_a are the quasiparticle energies and other terms of the hamiltonian are normal-ordered parts of the residual interaction labeled according to the number of quasiparticle creation and annihilation operators which they contain [14].

In the first version of the MQPM [8] the coupling part of the microscopic hamiltonian, H_{31}, does not emerge from the equations-of-motion method (EOM) [15]. The EOM

Table 1
Proton single-particle energies used in the MQPM calculations. The single-particle energies of the rest of the proton valence space are given in Fig. 1

s.p. orbital	^{135}I	^{137}Cs	^{139}La	^{141}Pr	^{143}Pm	^{145}Eu
$0f_{7/2}$	−12.289	−12.114	−11.945	−11.782	−11.619	−11.469
$0f_{5/2}$	−8.808	−8.694	−8.583	−8.476	−8.367	−8.269
$1p_{3/2}$	−7.597	−7.443	−7.294	−7.150	−7.005	−6.872
$1p_{1/2}$	−6.212	−6.083	−5.959	−5.838	−5.717	−5.618
$0g_{9/2}$	−5.402	−5.308	−5.217	−5.131	−5.043	−4.967
$0g_{7/2}$	0.000	0.000	0.000	0.000	0.000	0.000

Table 2
Neutron single-particle energies used in the MQPM calculations

s.p. orbital	^{135}I	^{137}Cs	^{139}La	^{141}Pr	^{143}Pm	^{145}Eu
$1d_{5/2}$	−7.192	−7.251	−7.302	−7.345	−7.382	−7.413
$0g_{7/2}$	−7.156	−7.283	−7.399	−7.504	−7.600	−7.688
$2s_{1/2}$	−5.402	−5.425	−5.443	−5.456	−5.466	−5.473
$1d_{3/2}$	−5.151	−5.203	−5.249	−5.289	−5.325	−5.356
$0h_{11/2}$	−4.226	−4.341	−4.444	−4.537	−4.621	−4.696
$1f_{7/2}$	0.000	0.000	0.000	0.000	0.000	0.000
$2p_{3/2}$	1.358	1.499	1.624	1.735	1.834	1.923
$0h_{9/2}$	1.724	1.602	1.488	1.379	1.275	1.176
$2p_{1/2}$	2.166	2.371	2.549	2.704	2.841	2.963
$1f_{5/2}$	2.715	2.792	2.853	2.903	2.945	2.979

method introduces an additional term into the quasiparticle-phonon matrix elements, not taken into account in Ref. [8]. In the present article we use the EOM form of the coupling part of the hamiltonian. In addition to being microscopically more justified, this form of the coupling hamiltonian yields results closer to the experimental data and thus improves the quantitative predictability of the MQPM.

In the MQPM calculation we use for the protons the 1p0f and 2s1d0g oscillator major shells supplemented by the $h_{11/2}$ intruder orbital from the next oscillator major shell. For the neutrons we use the 2s1d0$g_{7/2}$ and 2p1f0h valence space. The proton single-particle energies ε_α of Eq. (1) are taken to correspond to those of Fig. 1, i.e. we take the same relative spacing of the key orbitals as used in the shell model calculation. The single-particle energies of Fig. 1 are extracted from the experimental ^{133}Sb spectrum [16], with the exception of the $2s_{1/2}$ single-particle energy which has not yet been measured. We have used the same value for the $2s_{1/2}$ single-particle energy as in the work of Sagawa et al. [17]. The proton energies outside this set of states, as well as the neutron single-particle energies, we take from the Coulomb-corrected Woods–Saxon potential with the parametrization of Ref. [18]. These single-particle energies are displayed in Tables 1 and 2.

In the next step a correlated ground state and the excited states of the even–even reference nucleus are constructed by use of the QRPA. In the QRPA the creation

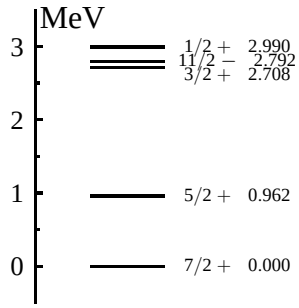

Fig. 1. Adopted single-particle energies for the proton orbitals $2s_{1/2}$, $1d_{3/2}$, $1d_{5/2}$, $0g_{7/2}$ and $h_{11/2}$ in the MQPM and the shell model calculation.

operator for an excited state (QRPA phonon) has the form

$$Q^{\dagger}_{\omega} = \sum_{a \leqslant a'} \left[X^{\omega}_{aa'} A^{\dagger}(aa'; J_{\omega} M) - Y^{\omega}_{aa'} \tilde{A}(aa'; J_{\omega} M) \right], \tag{4}$$

where the quasiparticle pair creation and annihilation operators are defined as $A^{\dagger}(aa'; JM) = \sigma^{-1}_{aa'} [a^{\dagger}_{a} a^{\dagger}_{a'}]_{JM}$, $\tilde{A}(aa'; JM) = \sigma^{-1}_{aa'} [\tilde{a}_{a} \tilde{a}_{a'}]_{JM}$ and $\sigma_{aa'} = (1 + \delta_{aa'})^{1/2}$. Here the greek indices ω denote phonon spin J and parity π. Furthermore, they contain an additional quantum number k enumerating the different QRPA roots for the same angular momentum and parity. Thus $\omega = \{J_{\omega}, \pi_{\omega}, k_{\omega}\}$.

For each value of the angular momentum and parity the spectrum of the even–even nucleus is constructed by diagonalizing the QRPA matrix containing the usual submatrices A (quasiparticle–quasiparticle interaction) and B (induced by correlations of the ground state) [13]. The basis states in our quasiparticle-phonon calculation are constructed from the previously determined BCS quasiparticles and the QRPA phonons. In the MQPM we make the following ansatz for the states in an even–odd nucleus

$$|i; jm\rangle = \left(\sum_{n} C^{i}_{n} a^{\dagger}_{njm} + \sum_{nj'\alpha} C^{i}_{nj'\alpha} [a^{\dagger}_{nj'} Q^{\dagger}_{\alpha}]_{jm} \right) |-\rangle, \tag{5}$$

where $|-\rangle$ denotes the QRPA vacuum of the even–even reference nucleus. The overlap matrix elements between the quasiparticle-phonon states and the matrix elements of the quasiparticle-phonon hamiltonian in this basis have the following form

$$\langle -|[a^{\dagger}_{n} Q^{\dagger}_{\alpha}]^{\dagger}_{j} [a^{\dagger}_{n'} Q^{\dagger}_{\alpha'}]_{j}|-\rangle = \delta_{\alpha\alpha'}\delta_{nn'} + A\left(\alpha n \alpha' n'; j\right),$$

$$\begin{aligned}
\langle -|[a^{\dagger}_{n} Q^{\dagger}_{\alpha}]^{\dagger}_{j} H [a^{\dagger}_{n'} Q^{\dagger}_{\alpha'}]_{j}|-\rangle = {} & \frac{1}{2}\left(\hbar\Omega_{\alpha} + E_{n} + \hbar\Omega_{\alpha'} + E_{n'}\right) \\
& \times \langle -|[a^{\dagger}_{n} Q^{\dagger}_{\alpha}]^{\dagger}_{j} [a^{\dagger}_{n'} Q^{\dagger}_{\alpha'}]_{j}|-\rangle \\
& + \frac{1}{2} \hat{j}_{\alpha} \hat{j}_{\alpha'} \sum_{a} \begin{Bmatrix} j_{n'} & j_{a} & J_{\alpha} \\ j_{n} & j & J_{\alpha'} \end{Bmatrix} \\
& \times \left(\hbar\Omega_{\alpha} - E_{n} + \hbar\Omega_{\alpha'} - E_{n'} - 2E_{a}\right)
\end{aligned}$$

$$\times \bar{X}^{\alpha}_{an'} \bar{X}^{\alpha'}_{an} \sigma^{-1}_{an} \sigma^{-1}_{an'}, + \frac{1}{2} \hat{J}_{\alpha} \hat{J}_{\alpha'} \sum_{a} \frac{\delta_{jj_a}}{\hat{j}^2} \bar{Y}^{\alpha}_{an} \bar{Y}^{\alpha'}_{an'}$$

$$\times \left(-\hbar\Omega_{\alpha} - E_n - \hbar\Omega_{\alpha'} - E_{n'} - 2E_a \right) \sigma^{-1}_{an} \sigma^{-1}_{an'}, \quad (6)$$

where Ω_{α} denote the QRPA-phonon energies, and

$$A\left(\alpha n \alpha' n'; j\right) = \hat{J}_{\alpha} \hat{J}_{\alpha'} \sum_{a} \left[\begin{Bmatrix} j_{n'} & j_a & J_{\alpha} \\ j_n & j & J_{\alpha'} \end{Bmatrix} \bar{X}^{\alpha}_{an'} \bar{X}^{\alpha'}_{an} + \frac{\delta_{jj_a}}{\hat{j}^2} \bar{Y}^{\alpha}_{an} \bar{Y}^{\alpha'}_{an'} \right] \sigma^{-1}_{an} \sigma^{-1}_{an'}. \quad (7)$$

Here $\bar{X}^{\alpha}_{aa'} \equiv X^{\alpha}_{aa'} - (-1)^{j_a + j_{a'} - J_{\alpha}} X^{\alpha}_{a'a}$. The same definition holds for $\bar{Y}$.

The interaction matrix elements between the one-quasiparticle and quasiparticle-phonon states have the following form:

$$\begin{aligned}
\langle - | [Q_{\alpha} a_n]_{jm} \hat{H} a^{\dagger}_{\nu'} | - \rangle = {} & \frac{1}{3} \frac{\hat{J}_{\alpha}}{\hat{j}_{n'}} \sum_{a \leqslant a'} H_{\mathrm{pp}}(aa'nn'J_{\alpha}) \left(u_a u_{a'} X^{\alpha}_{aa'} - v_a v_{a'} Y^{\alpha}_{aa'} \right) \sigma^{-1}_{aa'} \\
& - \frac{1}{3} \frac{\hat{J}_{\alpha}}{\hat{j}_{n'}} \sum_{a \leqslant a'} H_{\mathrm{hh}}(aa'nn'J_{\alpha}) \left(v_a v_{a'} X^{\alpha}_{aa'} - u_a u_{a'} Y^{\alpha}_{aa'} \right) \sigma^{-1}_{aa'} \\
& + \frac{1}{3} \frac{\hat{J}_{\alpha}}{\hat{j}_{n'}} \sum_{a \leqslant a'} H_{\mathrm{ph}}(aa'nn'J_{\alpha}) \left(u_a v_{a'} X^{\alpha}_{aa'} + v_a u_{a'} Y^{\alpha}_{aa'} \right) \sigma^{-1}_{aa'} \\
& - \frac{1}{3} \frac{\hat{J}_{\alpha}}{\hat{j}_{n'}} \sum_{a \leqslant a'} H_{\mathrm{hp}}(aa'nn'J_{\alpha}) \left(v_a u_{a'} X^{\alpha}_{aa'} + u_a v_{a'} Y^{\alpha}_{aa'} \right) \sigma^{-1}_{aa'},
\end{aligned} \quad (8)$$

where

$$H_{\mathrm{pp}}(nn'aa'J) = 2 v_n u_{n'} G(nn'aa'J), \quad (9)$$

$$H_{\mathrm{hh}}(nn'aa'J) = 2 u_n v_{n'} G(nn'aa'J), \quad (10)$$

$$H_{\mathrm{ph}}(nn'aa'J) = 2 v_n v_{n'} F(nn'aa'J) + 2 u_n u_{n'} F(n'naa'J) (-1)^{j_n + j_{n'} + J}, \quad (11)$$

$$H_{\mathrm{hp}}(nn'aa'J) = 2 u_n u_{n'} F(nn'aa'J) + 2 v_n v_{n'} F(n'naa'J) (-1)^{j_n + j_{n'} + J}. \quad (12)$$

In the previous version of our model [8] the second term in the quasiparticle-phonon matrix elements of the hamiltonian in Eq. (6) was missing. This additional term stems from the use of the equations-of-motion (EOM) method [15] when deriving the eigenvalue equation (13) below. It has an important effect on the location of the three-quasiparticle-type states relative to the one-quasiparticle-type ones, and it is essential for yielding theoretical results in agreement with data.

The overlap between the one-quasiparticle and the quasiparticle-phonon states is always zero. However, the overlap between two quasiparticle-phonon states can be non-zero and the quasiparticle-phonon states form a non-orthogonal over-complete basis set. The ansatz (5) leads to a generalized hermitian (or real and symmetric) eigenvalue problem which has the form [8]

$$\sum_j H_{ij} C_j^{(n)} = \lambda_n \sum_j S_{ij} C_j^{(n)}, \tag{13}$$

where $H_{ij} = \langle i|H|j\rangle$ and $S_{ij} = \langle i|j\rangle$ is the overlap matrix element between two basis states (one-quasiparticle or quasiparticle-phonon states). To solve this rather involved eigenvalue problem we adopt the method where we first solve the eigenvalue equation for the overlap matrix $\boldsymbol{S}$:

$$\sum_j S_{ij} u_j^{(k)} = n_k u_i^{(k)}. \tag{14}$$

The eigenvectors can be written in the basis $\{|i\rangle\}$ as

$$|\tilde{k}\rangle = \frac{1}{\sqrt{n_k}} \sum_i u_i^{(k)} |i\rangle. \tag{15}$$

They have the property of being mutually orthogonal, have a norm equal to unity and form a complete set after removing states having eigenvalue $n_k = 0$ (this removes the overcompleteness of the set $\{|i\rangle\}$).

Using the new orthogonal complete set of states (15) we can transform (13) to an ordinary real and symmetric eigenvalue problem of the form

$$\sum_j \langle \tilde{i}|H|\tilde{j}\rangle g_j^{(n)} = \lambda_n g_i^{(n)}, \tag{16}$$

where

$$\langle \tilde{i}|H|\tilde{j}\rangle = \frac{1}{\sqrt{n_i n_j}} \sum_{kl} u_k^{(i)*} \langle k|H|l\rangle u_l^{(j)}. \tag{17}$$

The coefficients of the eigenstates are calculated from the g coefficients in the following way:

$$C_i^n = \sum_k n_k^{-1/2} g_k^{(n)} u_i^{(k)}. \tag{18}$$

In practice one omits states having eigenvalue n_k less than some set upper limit ϵ.

In the present work we have constructed the odd-A isotones by adding a proton particle to the adjacent even $N = 82$ isotone. The even $N = 82$ isotones thus provide our quasiparticles and QRPA phonons to be used in the ansatz of Eq. (5). As a matter of fact, these phonons have already been constructed in our previous study of the $N = 82$ isotones [9]. In the diagonalization of the MQPM matrix of Eq. (13) we have used the 4–6 lowest QRPA phonons of multipolarity 2^+, 3^-, 4^+, 5^-, 6^+ and 7^-. This number of selected multipolarities is large enough to stabilize the spectrum of the odd isotones (see Ref. [8]) and is referring to the determination of the most relevant part of the three-quasiparticle hilbert space mentioned in the introduction.

In this context it is important to point out that no 0^+ phonons are used to produce the MQPM results discussed in Section 4, although in the first part of our work [9] the excited 0^+ states were discussed extensively. There are two reasons why we omit

the 0^+ phonons in the present MQPM calculation, namely, for the first, in the isotones ^{136}Xe and ^{138}Ba the calculated energies of the first excited 0^+ state, 0_2^+, is seen to be more than 1 MeV too low in comparison with the corresponding experimental energy. In fact, in the QRPA the 0_2^+ energy is lower than the 2_1^+ energy for these isotones. Thus the wave function of the 0_2^+ might not be adequately described and this particular phonon would produce two "spurious" low-energy excitations with spins $7/2^+$ and $5/2^+$ coming from the $0_2^+ \otimes 7/2^+$ and $0_2^+ \otimes 5/2^+$ quasiparticle-phonon couplings. Due to this unrealistic feature the 0^+ phonons are discarded in these isotones. Secondly, in the other isotopes under discussion the calculated energy of the 0_2^+ state is well above the energy of the 2_1^+ state (confirmed by the experimental data in the cases of ^{140}Ce, ^{142}Nd and ^{144}Sm) and calculations show that in this case the inclusion of the 0^+ phonons has only a negligible effect on the results presented in Section 4.

3. Effective interaction and the shell model

Here we will briefly sketch the theory of the effective interaction and the shell model (SM).

Our scheme to derive an effective interaction can be divided into three steps. First, one needs a free NN interaction V which is suitable for nuclear physics at low and intermediate energies. At present, the most viable approach seems to be the meson-exchange picture. Among the meson-exchange models, one of the more successful is the one-boson-exchange model of the Bonn group [19].

As the next step a reaction matrix G is introduced. In this way we overcome the problem that the NN potential has a strongly repulsive core which makes it unsuitable for perturbative approaches. In this work we have calculated the G-matrix using the so-called double-partitioning scheme; see Ref. [10] for a recent review.

The last step is to define a two-body interaction in terms of the G-matrix. We include all diagrams to third order in perturbation theory and sum the so-called folded diagrams to infinite order, an approach known as the folded diagram method (see, e.g., Refs. [9,10] for further details). This procedure is the best presently possible for computing the effective interaction microscopically, although difficulties and uncertainties still exist. In spite of this, the present procedure has been found to yield reasonable results for the shell-model effective interaction in earlier calculations.

Our basic approach in solving the many-body eigenvalue problem is the Lanczos algorithm. This is an iterative method which was first applied to nuclear physics problems by Whitehead [20]. The eigenstates are expanded in an m-scheme slater determinant basis, which implies that the dimension of the problem grows rapidly with increasing number of valence particles (see Table 3). The advantage of this representation is, however, the very efficient implementation of the computer code. This is a shell model calculation where no truncations of configurations are made. For more details of the shell model algorithm, see Ref. [21].

The model space for the shell model calculation and the effective interaction is defined

Table 3
Number of basis states for the shell model calculation of the $N = 82$ isotones, with the $1d_{5/2}$, $0g_{7/2}$, $1d_{3/2}$, $2s_{1/2}$ and $0h_{11/2}$ single particle orbitals

System	Dimension	System	Dimension	System	Dimension
^{134}Te	36	^{139}La	108 297	^{144}Sm	6 210 638
^{135}I	245	^{140}Ce	323 682	^{145}Eu	9 397 335
^{136}Xe	1504	^{141}Pr	828 422	^{146}Gd	12 655 280
^{137}Cs	7451	^{142}Nd	1 853 256	^{147}Tb	15 064 787
^{138}Ba	31 124	^{143}Pm	3 609 550	^{148}Dy	16 010 204

by the $N = 4$ oscillator shell $(1d_{5/2}, 0g_{7/2}, 1d_{3/2}, 2s_{1/2})$. In addition, we have included the intruder $0h_{11/2}$ orbital from the $N = 5$ oscillator shell. Our model space consists of the proton orbitals outside the ^{132}Sn core, ranging from the closed $Z = 50$, $N = 82$ core to the $Z = N = 82$ core. There are no neutron degrees of freedom involved in this model. These degrees of freedom are accounted for by the various terms of the perturbation expansion used to derive the effective interaction. The adopted single-particle spectrum is as displayed in Fig. 1.

Before we present our comparison between the shell model results and those obtained with the MQPM, we would like to draw the attention to differences between the two methods. From the discussion in Section 2 we recall that the MQPM method employs exactly the same G-matrix interaction as that used to derive the shell model effective interaction. The single-particle energies for protons in the orbitals $1d_{5/2}0g_{7/2}1d_{3/2}2s_{1/2}0h_{11/2}$ defining the shell model space are the same as those used in the MQPM. In addition, no phenomenological adjustments are made of the G-matrix in the MQPM approach. However, the reader should note that the single-particle basis for protons is larger for the MQPM, allowing thereby for proton core excitations across the $Z = 50$ shell gap. Secondly, neutrons are also active, yielding neutron core excitations across the $N = 82$ shell gap. This might become important for the description of some low-energy collective excitations of the even $N = 82$ isotones. In the shell model approach these degrees of freedom are supposed to be accounted for by terms included in the perturbative expansion of the effective interaction. Substantial differences in the two approaches may therefore reveal that such low-energy collective excitations are not accounted for in the shell model approach.

4. Results and discussion

In Tables 4–9 we present our results for the calculated energy spectra of the odd $N = 82$ isotones of interest in this article. In these tables we also present the available experimental data in the first two columns of the tables. It should noted that the spin assignments in the first column are experimental ones and the spins in parentheses are only tentative. The MQPM and the SM results are always presented in the last two columns of the tables. The three middle columns are reserved for presenting the results

concerning the extreme quasiparticle-phonon picture. In this picture the energy of the multiplet emerging from angular-momentum coupling of the nth phonon of spin J and parity π, J^{π}_{n}, with the single-quasiparticle state j^{π} is obtained by simply summing the phonon and the quasiparticle energies. The column "proposed config." lists the phonon-quasiparticle states [1] which are among the leading ones in the wave function of the MQPM.

In the first subsection below we discuss the differences between the extreme quasiparticle picture and the MPQM. Thereafter, the MQPM results are compared with the corresponding results obtained from an unrestricted shell model calculation with the orbitals $1d_{5/2}0g_{7/2}1d_{3/2}2s_{1/2}0h_{11/2}$ defining the shell model space, having in mind the discussion in Section 3.

4.1. Microscopic quasiparticle-phonon model

In the extreme quasiparticle-phonon picture the two energies, (E(phen) and E(calc) in Tables 4–9, are obtained in the following way. For the phenomenological energy, E(phen), we have taken the phonon energy from experiments (i.e. from the measured spectrum of the even–even $N = 82$ isotone with one less proton) and the quasiparticle energy was deduced from the proton single-particle energies of Fig. 1 using the BCS expression

$$E^{\mathrm{qp}}_{\alpha} = \sqrt{(\varepsilon_{\alpha} - \lambda_{\mathrm{p}})^2 + \Delta^2}, \tag{19}$$

where ε_{α} is the single-particle energy of the active proton orbital and λ_{p} is the chemical potential for the protons. The chemical potential we have taken simply to correspond to the energy of the last occupied proton orbital in the even–even $N = 82$ reference nuclei. One exception is the case of ^{141}Pr where in the corresponding reference nucleus ^{140}Ce the proton $g_{7/2}$ orbital is completely filled and the chemical potential thus lies somewhere between the $g_{7/2}$ and $d_{5/2}$ orbitals. In this case one can deduce the value of the chemical potential by using the above formula to reproduce the experimental energy difference between the $7/2^{+}$ and $5/2^{+}$ (single-quasiparticle) states in ^{141}Pr. The quantity Δ in Eq. (19) is the pairing gap and assumes the phenomenological value

$$\Delta = 12A^{-1/2}\ \mathrm{MeV}. \tag{20}$$

The calculated extreme quasiparticle-phonon energy, E(calc), was obtained by summing the QRPA-calculated energy (see Ref. [9]) of the J^{π} phonons of the even reference nuclei with the single-quasiparticle energy coming from the BCS calculation.

In the following we shall comment on the MQPM results shown in Tables 4–9. The emphasis lies on analyzing the lowest-lying quasiparticle-phonon multiplets of the odd isotones with respect to their span in energy, their centroids and the relative location of the various spins within the perturbed multiplet. The multiplet of the extreme

[1] In the extreme quasiparticle-phonon picture we assume that only the proton-quasiparticle states are active in the low-energy spectrum of the odd isotones.

Table 4
Low-lying states for ^{135}I. Experimental angular momentum values in parentheses are tentative. Energies are given in MeV. The symbol sqp in the leading configuration column denotes a single-quasiparticle state. For further information concerning the extreme qp-phonon picture, see the text

		Extreme qp-phonon picture				
J^π	E(exp)	Proposed config.	E(phen)	E(calc)	E(MQPM)	E(SM)
$7/2^+$	0.000	$7/2^+$(sqp)	0.00	0.00	0.000	0.000
$(5/2^+)$	0.604	$5/2^+$(sqp)	0.38	0.70	0.649	0.508
$(5/2^+)$	0.870	$2_1^+ \otimes 7/2^+$	1.28	1.51	1.405	0.888
		$2_1^+ \otimes 7/2^+$	1.28	1.51	$1.498(9/2^+)$	$1.349(9/2^+)$
		$2_1^+ \otimes 7/2^+$	1.28	1.51	$1.533(3/2^+)$	$1.053(3/2^+)$
$11/2^+$	1.134	$2_1^+ \otimes 7/2^+$	1.28	1.51	1.543	1.322
		$2_1^+ \otimes 7/2^+$	1.28	1.51	$1.560(7/2^+)$	$1.619(7/2^+)$
$15/2^+$	1.422	$4_1^+ \otimes 7/2^+$	1.57	1.85	1.886	1.683
$17/2^+$	1.994	$6_1^+ \otimes 7/2^+$	1.69	1.94	2.033	1.966

Table 5
Low-lying states of ^{137}Cs. Legend as in Table 4

		Extreme qp-phonon picture				
J^π	E(exp)	Proposed config.	E(phen)	E(calc)	E(MQPM)	E(SM)
$7/2^+$	0.000	$7/2^+$(sqp)	0.00	0.00	0.000	0.000
$5/2^+$	0.456	$5/2^+$(sqp)	0.38	0.45	0.404	0.208
		$2_1^+ \otimes 7/2^+$	1.31	1.50	$1.315(5/2^+)$	$0.994(5/2^+)$
		$2_1^+ \otimes 7/2^+$	1.31	1.50	$1.471(9/2^+)$	$1.463(9/2^+)$
		$2_1^+ \otimes 7/2^+$	1.31	1.50	$1.512(3/2^+)$	$1.233(3/2^+)$
		$2_1^+ \otimes 7/2^+$	1.31	1.50	$1.529(7/2^+)$	$1.519(7/2^+)$
		$2_1^+ \otimes 7/2^+$	1.31	1.50	$1.530(11/2^+)$	$1.422(11/2^+)$
$1/2^+$	1.490	$2_1^+ \otimes 5/2^+$, $4_1^+ \otimes 7/2^+$	1.69	1.95–1.96	1.923	1.361
$9/2^-$	1.868	$2_1^+ \otimes 11/2^-$, $3_1^- \otimes 7/2^+$	3.26–3.27	3.10–3.62	3.126	2.061
$1/2^+$	2.150	$1/2^+$(sqp)	2.13	2.23	1.986	2.093

quasiparticle-phonon picture loses its energy degeneracy through the action of the residual interactions and the resulting multiplet we call a perturbed one. It is of interest to see how the breaking of the degeneracy evolves from nucleus to nucleus and what its characteristic features are.

We start first by noticing that the residual interactions yield relatively little perturbation on the energies of the single-quasiparticle-type states (denoted by the symbol (sqp) in the tables) in the MQPM calculation. The agreement in the single-quasiparticle energies between the MQPM and experiment is good due to the success of the BCS calculation in describing the lowest excitations of the odd isotones. This, in turn, means that the phenomenological mean field, represented by the proton single-particle energies of Fig. 1, is consistent with the residual pairing interactions used in the present calculation.

As a general feature of the MQPM results one can say that the MQPM describes better the heavier $N = 82$ isotones (both even [9] and odd) since the heavier isotones are not in the immediate vicinity of the $Z = 50$ closed core and thus the quasiparticle

Table 6
Low-lying states of ^{139}La. Legend as in Table 4. The underlined spin assignments are considered to be favoured by the SM and the MQPM calculations

		Extreme qp-phonon picture				
J^π	E(exp)	Proposed config.	E(phen)	E(calc)	E(MQPM)	E(SM)
$7/2^+$	0.000	$7/2^+$(sqp)	0.00	0.00	0.000	0.000
$5/2^+$	0.166	$5/2^+$(sqp)	0.38	0.19	0.154	0.061
$1/2^+$	1.209	$2_1^+ \otimes 5/2^+$	1.82	1.69	1.633	1.331
		$(4_1^+ \otimes 7/2^+)$	(1.90)	(2.08)		
$9/2^+$	1.219	$2_1^+ \otimes 7/2^+$	1.44	1.50	1.451	1.432
$(5/2)^+$	1.257	$2_1^+ \otimes 7/2^+$	1.44	1.50	1.256	0.983
$(9/2^+)$	1.381	$2_1^+ \otimes 5/2^+$	1.82	1.69	1.719	1.491
$(11/2)^-$	1.420	$11/2^-$(sqp)	1.95	1.71	1.660	1.770
$\underline{5/2^+}, 7/2^+$	1.421	$2_1^+ \otimes 5/2^+$	1.82	1.69	1.644	1.467
$\underline{(9/2^+)}$	1.476	$4_1^+ \otimes 7/2^+$	1.90	2.08	2.068	1.818
$11/2^+$	1.534	$2_1^+ \otimes 7/2^+$	1.44	1.50	1.530	1.389
$7/2^+$	1.538	$2_1^+ \otimes 7/2^+$	1.44	1.50	1.462	1.530
$\underline{3/2^+}, 5/2^+$	1.558	$2_1^+ \otimes 7/2^+$	1.44	1.50	1.495	1.037
$\underline{(15/2)^-}$	3.375	$2_1^+ \otimes 11/2^-$	3.39	3.21	3.242	3.193
$17/2^-$	3.927	$4_1^+ \otimes 11/2^-$	3.85	3.79	3.311	3.798

Table 7
Low-lying states of ^{141}Pr. Legend as in Table 4

		Extreme qp-phonon picture				
J^π	E(exp)	Proposed config.	E(phen)	E(calc)	E(MQPM)	E(SM)
$5/2^+$	0.000	$5/2^+$(sqp)	0.00	0.00	0.000	0.000
$7/2^+$	0.145	$7/2^+$(sqp)	0.145[a]	0.072	0.104	0.008
$11/2^-$	1.118	$11/2^-$(sqp)	1.31	1.31	1.301	1.497
$3/2^+$	1.127	$2_1^+ \otimes 5/2^+$	1.60	1.48	1.314	0.936
$(5/2)^+$	1.293	$2_1^+ \otimes 5/2^+$	1.60	1.48	1.371	0.993
$1/2^+$	1.299	$1/2^+$(sqp)	1.49	1.42	1.396	1.148
$3/2^+$	1.436	$3/2^+$(sqp)	1.23	1.30	1.342	1.140
$(7/2)^+$	1.452	$2_1^+ \otimes 5/2^+$	1.60	1.48	1.440	1.452
$9/2^+$	1.457	$2_1^+ \otimes 5/2^+$	1.60	1.48	1.522	1.413
$11/2^+$	1.494	$2_1^+ \otimes 7/2^+$	1.74	1.55	1.622	1.418
$9/2^+$	1.521	$2_1^+ \otimes 7/2^+$	1.74	1.55	1.549	1.413
$(3/2)^+$	1.608	$2_1^+ \otimes 7/2^+$	1.74	1.55	1.626	1.372
$1/2^+$	1.658	$2_1^+ \otimes 5/2^+$	1.60	1.48	1.602	1.545
$13/2^+$	1.768	$4_1^+ \otimes 5/2^+$	2.08	2.14	2.206	1.939
$15/2^+$	1.797	$6_1^+ \otimes 5/2^+$	2.11	2.21	2.278	1.978
$13/2^+$	1.986	$6_1^+ \otimes 5/2^+$	2.11	2.21	2.206	2.004
$17/2^+$	2.070	$6_1^+ \otimes 5/2^+$	2.11	2.21	2.280	2.064

[a]The chemical potential of Eq. (19) was fixed by the experimental quasiparticle energy.

description is expected to be better justified.

For ^{135}I the wrong theoretical 2_1^+ energy in ^{134}Te (see Ref. [9]) leads to too high an energy for the multiplet $2_1^+ \otimes 7/2^+$ (see Table 4) and thus to too high an energy for the associated MQPM states (i.e. to too high a centroid of the MQPM multiplet).

Table 8
Low-lying states of ^{143}Pm. Legend as in Table 4. The underlined spin assignments are considered to be favoured by the SM and the MQPM calculations

		Extreme qp-phonon picture				
J^π	E(exp)	Proposed config.	E(phen)	E(calc)	E(MQPM)	E(SM)
$5/2^+$	0.000	$5/2^+$(sqp)	0.00	0.00	0.000	0.000
$7/2^+$	0.272	$7/2^+$(sqp)	0.39	0.32	0.342	0.003
$11/2^-$	0.960	$11/2^-$(sqp)	1.08	1.01	1.009	1.203
$3/2^+$	1.060	$3/2^+$(sqp)	1.01	1.06	1.088	0.728
$1/2^+$	1.173	$1/2^+$(sqp)	1.26	1.14	1.166	0.731
$(\underline{3/2}, 5/2)$	1.287	$2_1^+ \otimes 5/2^+$	1.58	1.46	1.176	1.391
$\underline{3/2^+}$	1.403	$2_1^+ \otimes 7/2^+$	1.96	1.79	1.854	
$9/2^+$	1.456	$2_1^+ \otimes 5/2^+$	1.58	1.46	1.531	1.512
$3/2^+, \underline{5/2^+}$	1.515	$2_1^+ \otimes 5/2^+$	1.58	1.46	1.524	1.325
$(5/2^+)$	1.566	$2_1^+ \otimes 5/2^+$	1.58	1.46	$1.521(7/2^+)$	$1.430(7/2^+)$
$(9/2)^+$	1.566	$2_1^+ \otimes 7/2^+$	1.96	1.79	1.747	
$3/2^+, \underline{5/2^+}$	1.614	$2_1^+ \otimes 7/2^+$	1.96	1.79	1.680	1.403
$11/2^+$	1.664	$2_1^+ \otimes 7/2^+$	1.96	1.79	1.854	
$1/2^+$	1.753	$2_1^+ \otimes 5/2^+$	1.58	1.46	1.537	1.632
$15/2^+$	1.898	$4_1^+ \otimes 7/2^+$	2.49	2.46	2.528	
$17/2^+$	2.288	$6_1^+ \otimes 5/2^+$	2.21	2.36	2.432	

The same is valid for the 4_1^+ energy and the associated $4_1^+ \otimes 7/2^+$ multiplet. For the other even reference isotones the phonon energies of the $2_1^+, 3_1^-, 4_1^+$ and 6_1^+ states are in reasonable agreement with experiment and in the case of ^{138}Ba, ^{140}Ce and ^{142}Nd the agreement is rather good [9].

Let us now discuss the lowest observed multiplets of the odd isotones, namely $2_1^+ \otimes 7/2^+$ for $A = 139$ and $2_1^+ \otimes 5/2^+$ for $A = 141, 143$, as well as $3_1^- \otimes 5/2^+$ for ^{145}Eu. Since experimental data on the $2_1^+ \otimes 7/2^+$ multiplet are missing or incomplete for ^{135}I and ^{137}Cs, only ^{139}La is left for comparison. From Table 6 one observes that the experimental and the MQPM centroids correspond to each other rather nicely and the width of both spectra is the same. In addition, the $3/2^+$, $5/2^+$, $7/2^+$ and $11/2^+$ members of the multiplet are reproduced by the MQPM rather well but the MQPM clearly fails for the $9/2^+$ state. In this case the phenomenological quasiparticle-phonon energy E(phen) = 1.44 MeV is more or less the centroid of both the experimental and the MQPM multiplet. The corresponding calculated energy E(calc) = 1.50 MeV is slightly higher.

The above described features are also seen in the $2_1^+ \otimes 7/2^+$ multiplet in ^{141}Pr, where this multiplet is no longer the lowest one but above the $2_1^+ \otimes 5/2^+$ multiplet (see Table 7). A clear agreement of the MQPM with the data, especially in the case of the $3/2^+$ member of the multiplet, is evident.

The same type of analysis can be performed for the $2_1^+ \otimes 5/2^+$ multiplet which is the lowest in ^{141}Pr and ^{143}Pm (see Tables 7 and 8). In Table 7 it is seen that for ^{141}Pr the centroid of the experimental multiplet is well reproduced by the MQPM as is also the case for ^{143}Pm. A closer look at the spectrum of ^{141}Pr reveals that the $3/2^+$

Table 9
Low-lying states of ^{145}Eu. Legend as in Table 4. In this case only the MQPM results are available since the SM calculations are already beyond any reasonable effort

J^π	E(exp)	Extreme qp-phonon picture			E(MQPM)
		Proposed configuration(s)	E(phen)	E(calc)	
$5/2^+$	0.000	$5/2^+$(sqp)	0.00	0.00	0.000
$7/2^+$	0.329	$7/2^+$(sqp)	0.39	0.54	0.551
$11/2^-$	0.716	$11/2^-$(sqp)	1.08	0.60	0.618
$1/2^+$	0.809	$1/2^+$(sqp)	1.26	0.76	0.788
$3/2^+$	1.042	$3/2^+$(sqp)	1.01	0.71	0.737
$9/2^-$	1.368	$3_1^- \otimes 5/2^+$	1.81	1.48	1.542
$1/2^+$	1.460	$2_1^+ \otimes 5/2^+$	1.66	1.48	1.547
$7/2^-$	1.500	$3_1^- \otimes 5/2^+$	1.81	1.48	1.541
		$3_1^- \otimes 5/2^+$	1.81	1.48	$1.532(1/2^-)$
$3/2^-$,$5/2^-$	1.567	$3_1^- \otimes 5/2^+$	1.81	1.48	$1.542(5/2^-)$
$3/2^-$	1.600	$3_1^- \otimes 5/2^+$	1.81	1.48	1.535
$11/2^-$	1.602	$3_1^- \otimes 5/2^+$	1.81	1.48	1.553
		$2_1^+ \otimes 5/2^+$	1.66	1.48	$1.543(9/2^+)$
		$2_1^+ \otimes 5/2^+$	1.66	1.48	$1.571(7/2^+)$
		$2_1^+ \otimes 5/2^+$	1.66	1.48	$1.587(5/2^+)$
$7/2^-$	1.745	$3_1^- \otimes 7/2^+$, $2_1^+ \otimes 11/2^-$	2.20,2.57	2.02,2.08	2.080
$3/2^+$	1.758	$2_1^+ \otimes 5/2^+$	1.66	1.48	1.258
$3/2^-$	1.762	$3_1^- \otimes 7/2^+$	2.20	2.02	2.070
$5/2^-$	1.766	$3_1^- \otimes 7/2^+$	2.20	2.02	2.065
$11/2^-$	1.792	$3_1^- \otimes 7/2^+$, $2_1^+ \otimes 11/2^-$	2.20,2.57	2.02,2.08	2.084
$9/2^-$	1.827	$3_1^- \otimes 7/2^+$, $2_1^+ \otimes 11/2^-$	2.20,2.57	2.02,2.08	2.084
		$2_1^+ \otimes 7/2^+$, $3_1^- \otimes 11/2^-$	2.05,2.89	2.02,2.07	$1.928(7/2^+)$
$3/2^+$,$5/2^+$	1.845	$2_1^+ \otimes 7/2^+$, $3_1^- \otimes 11/2^-$	2.05,2.89	2.02,2.07	$1.952(5/2^+)$
		$2_1^+ \otimes 7/2^+$, $3_1^- \otimes 11/2^-$	2.05,2.89	2.02,2.07	$1.977(9/2^+)$
$1/2^+$,$3/2^+$	1.881	$2_2^+ \otimes 5/2^+$	2.42	2.58	$2.090(1/2^+)$
$(3/2,5/2)^+$	1.915	$2_1^+ \otimes 7/2^+$, $3_1^- \otimes 11/2^-$	2.05,2.89	2.02,2.07	$2.161(5/2^+)$
$3/2^+$	2.049	$2_1^+ \otimes 7/2^+$	2.05	2.02	2.295
$5/2^+$	2.114	$2_1^+ \otimes 7/2^+$	2.05	2.02	2.252
$9/2^-$,$11/2^-$	2.117	$3_1^- \otimes 7/2^+$, $2_1^+ \otimes 11/2^-$	2.20,2.57	2.02,2.08	$2.095(9/2^-)$

and $9/2^+$ states are too far away from the $7/2^+$ state and the states are more homogeneously distributed in the theoretical spectrum. The undisturbed quasiparticle-phonon energies, E(phen) and E(calc), lie near the top of the experimental and theoretical multiplet, respectively. This situation is reversed in the case of ^{143}Pm, namely now the experimental multiplet is more homogeneously distributed and the MQPM fails in predicting the location of the $9/2^+$ state whereas for the other members of the multiplet the MQPM energies roughly correspond to the experimental ones even though the $5/2^+$ and $7/2^+$ states are inverted in the theory. Once again the undisturbed quasiparticle-phonon energies are near the top of the perturbed multiplet.

Finally, in Table 9 one can observe the lowest multiplet, $3_1^- \otimes 5/2^+$, of ^{145}Eu. One can see that the centroid of the calculated multiplet is more or less correct but that the multiplet is far too compressed when compared with the experimental span of the multiplet (in experiment the $9/2^-$ state comes very much down in energy). It seems that

in the MQPM the biggest qualitative and quantitative problems appear for the $3/2^-$ and $9/2^-$ members of the multiplet. It should be noted that in Table 9 the labelling of the higher excited states by the extreme quasiparticle-phonon wave function is to be taken with a grain of salt since many of the MQPM states at these energies can be constructed by superposition of a large number of possible quasiparticle-phonon components lying roughly in the same energy region. Thus the overlap of the proposed quasiparticle-phonon structures of Table 9 with the MQPM wavefunctions is not necessarily very big. The assignments may be considered more as a means of keeping track of the experimental states with the same spin.

As stated earlier, the spreading of the multiplet of the extreme quasiparticle-phonon picture can be ascribed to the influence of the residual interactions, coming mainly from the H_{31} part of the residual hamiltonian. This spreading in energy ranges roughly from 100 to 400 keV in the discussed odd isotones and the calculated extreme quasiparticle-phonon energy (E(calc) in the tables) lies rather close to the top of the perturbed multiplet. This means that the residual interactions tend to redistribute the multiplet energies towards lower energies (the centroid of the perturbed multiplet is always substantially lower than the extreme quasiparticle-phonon energy).

It should also be noted that in the MQPM calculation the energies of the $3/2^+$ and $9/2^+$ members of the $2_1^+ \otimes 7/2^+$ multiplet are the ones least affected by the residual interactions in the case of ^{135}I, ^{137}Cs, ^{139}La and ^{141}Pr. For the $2_1^+ \otimes 5/2^+$ multiplet all the spin members of the multiplet are clearly affected by the residual interaction, some of them considerably. The most strongly affected member of the $2_1^+ \otimes 7/2^+$ multiplet is the $5/2^+$ state whereas the $3/2^+$ state is most affected in the $2_1^+ \otimes 5/2^+$ multiplet.

4.2. Comparison with shell model results

In the MQPM scheme one starts with the BCS occupation probabilities stemming from the even isotones, given in Ref. [9]. As discussed in Section 2, the residual many-body hamiltonian can be expressed in terms of these occupation probabilities. In general, for the single-particle states we obtained good agreement in Ref. [9] between the shell model occupation probabilities and those of a BCS calculation for the even isotones. Since the states of the MQPM, shown in Tables 4–9, are combinations of single-particle states and phonons from the corresponding even isotones, it is then of interest to see whether one can retrace eventual discrepancies between the shell model approach and the MQPM to the fact that the SM employs a smaller set of single-particle orbitals in the diagonalization than the MQPM. It is therefore important to see how a renormalized effective interaction obtained by perturbative many-body methods is able to account for degrees of freedom not accounted for by the SM model space. It is, however, important to notice that although the MQPM employs a larger set of single-particle orbitals, only a limited set of states are obtained from the diagonalizations. In the SM all states are, in principle, taken into account in the diagonalization.

The shell model results are presented in Tables 4–8. In general, there is a fairly good agreement between the shell model results and experiment, with deviations of the order

Table 10
Lowest-lying states of given multipolarity in ^{141}Pr using various approximations to the effective interaction

J^π	E(exp)	E(BCS-1)	E(BCS-2)	E(MQPM)	$E(G)$	E(SM)
$5/2^+$	0.000	0.17	0.00	0.00	0.00	0.000
$7/2^+$	0.145	0.00	0.07	0.104	0.034	0.008
$11/2^-$	1.118	1.42	1.31	1.301	0.889	1.497
$3/2^+$	1.127	1.44	1.30	1.314	0.915	0.936
$1/2^+$	1.299	1.58	1.42	1.396	1.292	1.148

of 100–300 keV. However, as the number of valence particles increases from three in ^{135}I to 13 in ^{143}Pm, the description of the spacing between the lowest-lying $5/2^+$ and $7/2^+$ states becomes worse.

In order to understand these differences we have performed additional shell model calculations for ^{141}Pr with just the G-matrix as effective interaction, in order to see whether different approaches to the effective interaction within the $2s1d0g_{7/2}0h_{11/2}$ model space yield significant discrepancies. These results are displayed in Table 10, under the column labelled $E(G)$. The shell model results with the effective interaction to third-order in G from Table 7, together with the corresponding MQPM results, are included for comparison. These are labelled E(SM) and E(MQPM), respectively.

One can see from Table 10 that when going from the third-order effective interaction over to the bare G-matrix interaction in the shell model, the spacing between the lowest-lying $5/2^+$ and $7/2^+$ states increases to 0.034 MeV, although it is still far from the experimental value. The spectrum of the other states is more compressed than for the E(SM) results. The proton occupation numbers also change, but all states of ^{141}Pr are still strongly dominated by admixtures from the $5/2^+$ and $7/2^+$ single-particle states.

The question then arises whether these differences can be traced back to the use of a smaller model space in the shell model calculation. We have therefore performed a BCS calculation in the model-space defined by the $2s1d0g_{7/2}0h_{11/2}$ single-particle orbitals, using the G-matrix as interaction and the single-particle energies of Fig. 1. These results are labelled E(BCS-1) in Table 10. It should be noted that in this BCS calculation the mean-field part is the same as in the $E(G)$ calculation but that a BCS calculation includes only a very restricted set of states as compared to the full shell model diagonalization. The comparison reveals then how good or bad the BCS approximation is. As stated earlier, the BCS calculation forms the basis for the MQPM method. Moreover, the MQPM method used here employs a larger single-particle basis than that used in the shell model calculation or the BCS-1 calculation. It may therefore be of interest to see how the BCS calculation changes when we go to the model space employed in the MQPM calculation. The results of such a BCS calculation are denoted by E(BCS-2) in Table 10.

One can see from Table 10 that the results of the BCS-1 calculation clearly deviate from the BCS-2 results, indicating the importance of a larger single-particle basis. The relative positions of the $5/2^+$ and $7/2^+$ states are inverted and the other states are

Table 11
Squared overlaps $|\langle j^\pi; \mathrm{SM}(A)|a_j^\dagger|0^+; \mathrm{SM}(A-1)\rangle|^2$ for the SM and one-quasiparticle probabilities for the MQPM

J^π	^{135}I		^{137}Cs		^{139}La		^{141}Pr		^{143}Pm	
	SM	MQPM	SM	MQPM	SM	MQPM	SM	MQPM	SM	MQPM
$7/2_1^+$	0.99	0.99	0.99	0.99	0.98	0.99	0.97	0.99	0.95	0.99
$5/2_1^+$	0.94	0.98	0.95	0.98	0.95	0.99	0.94	0.98	0.98	0.98
$3/2_1^+$	0.00	0.01	0.01	0.03	0.07	0.19	0.12	0.45	0.89	0.97
$3/2_2^+$	0.00	0.00	0.09	0.00	0.02	0.00	0.75	0.52	0.00	0.01
$1/2_1^+$	0.11	0.00	0.11	0.15	0.29	0.32	0.89	0.73	0.90	0.97
$11/2_1^-$	0.98	0.94	0.96	0.95	0.94	0.95	0.91	0.96	0.89	0.96

higher in excitation energy in the BCS-1 calculation. Comparing the BCS-1 results with the $E(G)$ results, which are actually in reasonable agreement with experiment, clearly indicates that the simple BCS picture is far from sufficient in the restricted $2s1d0g_{7/2}0h_{11/2}$ valence space. The BCS-2 calculation, which employs the larger set of single-particle states, yields results which are closer to experiment and close to the MQPM results. The mere difference between the BCS-2 and MQPM results is in the better reproduction of the $5/2^+ - 7/2^+$ spacing by the MQPM.

In summary, the results in Table 10 seem to indicate that degrees of freedom not accounted for by the model space employed in the shell model calculation are important in order to obtain a proper reproduction of the experimental spacing between the two lowest-lying $5/2^+$ and $7/2^+$ states. However, when comparing the BCS-1 results with those of a shell model calculation with the bare G-matrix, one sees that there are important differences. Sources of these discrepancies are the many-body configurations not accounted for by the BCS approach. How these differences will appear in a shell model calculation which would employ the same set of single-particle energies as the BCS-2 or MQPM approaches is however not clear.

In column three of Tables 4–9 we indicate the MQPM states that are supposed to be of single-quasiparticle nature. For comparison with the shell model we create single-quasiparticle states for the odd-nucleon system by coupling a (j^π) particle to the 0^+ ground state of the neighbouring $A-1$ even system, $a_j^\dagger|\mathrm{SM}(A-1)\rangle$. By calculating the squared overlap between the constructed single-quasiparticle state and the SM state, $|\langle j^\pi; \mathrm{SM}(A)|a_j^\dagger|0^+; \mathrm{SM}(A-1)\rangle|^2$, we obtain a measure of the fraction of single-quasiparticle structure in our SM wave function. The results are tabulated in Table 11. There is a nice correspondence between the MQPM states proposed to be of single-quasiparticle nature and those SM states with predominantly single-quasiparticle structure. In the case of the $3/2_1^+$ and $3/2_2^+$ states in ^{141}Pr there is a strong mixing of the one- and three-quasiparticle components in the MQPM, stronger than in the SM. Squared overlaps of magnitudes 0.95–1.00 confirm that the $5/2_1^+$ and the $7/2_1^+$ states are fairly pure single-quasiparticle states.

We then turn to a comparison of the predominantly three-quasiparticle states in the two models. For this we consider the multiplets $2_1^+ \otimes 7/2^+$ for $A = 135, 137, 139$ and

$2_1^+ \otimes 5/2^+$ for $A = 141, 143$. We start with the $2_1^+ \otimes 7/2^+$ multiplet. Looking at Tables 4–6 one can see differences in the SM and the MQPM spectra of states ($3/2^+$, $5/2^+$, $7/2^+$, $9/2^+$, $11/2^+$) belonging to this multiplet. Characteristic features are (1) the centroid of the SM multiplet is always lower than the centroid of the MQPM multiplet; (2) the high-spin members of the multiplet ($7/2^+$, $9/2^+$, $11/2^+$) correspond quite well to each other in the SM and the MQPM, whereas the $5/2^+$ member of the multiplet is consistently lower in the SM spectra than in the MQPM spectra (in both cases the $5/2^+$ state is usually the lowest one); (3) differences show up for the lowest-spin member of the multiplet, i.e. for spin $3/2^+$, which is always the second lowest in energy in the SM spectra but among the three highest levels in the MQPM spectra.

The above listed properties of the SM and the MQPM spectra distinguish between the two calculations. For ^{135}I and ^{137}Cs the data are missing or incomplete so that essentially only ^{139}La is left for comparison. From Table 6 one observes that the experimental and the MQPM centroids correspond to each other rather nicely and the width of both spectra is the same. In addition, the $3/2^+$, $5/2^+$, $7/2^+$ and $11/2^+$ members of the multiplet are reproduced by the MQPM rather well (both the SM and the MQPM fail for the $9/2^+$ state), whereas in the case of the SM large deviations are observed for the $5/2^+$ member and especially for the $3/2^+$ member of the multiplet. Thus the experiment favours the MQPM sequence of levels in the $2_1^+ \otimes 7/2^+$ multiplet (although also in the MQPM the sequence of levels is not completely correct). For the $2_1^+ \otimes 7/2^+$ multiplet in ^{141}Pr (see Table 7) the differences between the two models and the experimental data are small.

The same type of analysis can be performed for the $2_1^+ \otimes 5/2^+$ multiplet which is the lowest in ^{141}Pr and ^{143}Pm (see Tables 7 and 8). In this case the differences between the SM and the MQPM spectra are less than for the $2_1^+ \otimes 7/2^+$ case. For ^{141}Pr the centroid of the experimental multiplet is well reproduced by the MQPM, clearly better than by the SM, whereas for ^{143}Pm both the SM and the MQPM have roughly the correct centroid. The largest difference between the SM and the MQPM spectra is found in the location of the $5/2^+$ member of the multiplet and the experimental data favours the MQPM for the $5/2^+$ energy.

4.3. Comparison with the results of Heyde and Waroquier

Finally, we want to say a few words about the comparison of our results with those of Heyde and Waroquier [12]. In Ref. [12] results for positive-parity and $11/2^-$ states of the odd isotones $A = 137$–145 are given. As already mentioned in the Introduction, we perform here only a brief qualitative comparison since the hamiltonian of Ref. [12] and the hamiltonians of the MQPM and SM are not directly comparable with each other. The single-quasiparticle energies were fitted in Ref. [12] by the use of the inverse-gap-equation method, and this yields the energies of the single-quasiparticle states of Ref. [12] generally better in agreement with experiment than the corresponding energies of the MQPM or the SM. There are, however, also situations where the reverse happens, i.e. for some of the single-quasiparticle states proposed in Tables 4–9 the MQPM reproduces the experimental energies better than in Ref. [12].

For the three-quasiparticle states the MQPM and the SM give, on average, better results than Ref. [12] for the isotones ^{139}La, ^{141}Pr and ^{143}Pm. In the case of the few positive-parity states of Table 9 in ^{145}Eu the MQPM and Ref. [12] give results of the same quality but Ref. [12] does not give any predictions for the many negative-parity states listed in Table 9. For ^{137}Cs it is not easy to make any comparison due to the scarce experimental information on the excitation spectrum.

5. Conclusions

The present work discusses the theoretical interpretation of low-energy excitations of odd $N = 82$ isotones between mass numbers $A = 135$ and $A = 143$. The energy spectra of these isotones have been calculated by using the microscopic quasiparticle-phonon model (MQPM) and the results have been compared with the extreme quasiparticle-phonon picture and the results of a large-basis shell model calculation with 3–11 valence protons outside the doubly-magic ^{132}Sn core. This work is a direct continuation of our earlier work on even $N = 82$ isotones [9] and the same realistic, microscopic two-body G-matrix interaction has been used in the present MQPM calculation as was used in the QRPA calculation of the even isotones (in fact, the QRPA calculation is a necessary prerequisite of the present MQPM calculation). Also in the shell model calculation we use the same effective two-body matrix elements, derived from the above-mentioned G-matrix elements through many-body perturbation techniques, which were used for the even isotones.

Overall, the spectra of the odd isotones are described well by the MQPM considering that no fitting of the interaction was done. This feature may be traced back to the capability of the BCS approach in describing excitations of one-quasiparticle type. From this one can conclude that the pairing-type of residual interactions used in the MQPM are consistent with the mean field extracted from the experimental single-particle energies in ^{133}Sb. The low-lying experimental levels can be labeled by their assumed leading quasiparticle-phonon contributions and their energies can be compared with the energies of the unperturbed quasiparticle-phonon multiplets and the perturbed ones emerging from the MQPM calculations. In the MQPM both the widths and the centroids of the perturbed multiplets, as well as the sequences of different spins within the multiplets, are described rather nicely. The shell model describes most individual states very well, in many cases better than the MQPM, but has difficulties in describing the centroids of the quasiparticle-phonon multiplets and energies of some members of these multiplets, particularly the $3/2^+$ states in the $2_1^+ \otimes 7/2^+$ multiplets and the $5/2^+$ states in the $2_1^+ \otimes 5/2^+$ multiplets.

The aim of the present work was to see how well a microscopic model, based on quasiparticle-phonon coupling and realistic microscopic G-matrix interactions, can describe the level systematics of a set of heavy semi-magic nuclei. At the same time the results of these calculations can be compared with results coming from a large-scale shell model calculation with microscopic effective interaction based on the same

G-matrix which is used in the quasiparticle-phonon calculation. Considering that in both calculations only very few parameters enter the calculation, the success of both models is surprisingly good.

Acknowledgements

This work was supported by the NorFA (Nordic Academy for Advanced Study). Support from the Research Council of Norway (Programme for Supercomputing) is also acknowledged. J.S. and J.T. acknowledge the financial support of the Academy of Finland (contract no. 35961).

References

[1] L.S. Kisslinger and R.A. Sorensen, Rev. Mod. Phys. 35 (1963) 853.
[2] J.A. Halbleib and R.A. Sorensen, Nucl. Phys. A 98 (1967) 542.
[3] G.J. Dreiss et al., Phys. Rev. C 3 (1971) 2412.
[4] W.F. van Gunsteren, E. Boeker and K. Allaart, Z. Phys. A 267 (1974) 87;
W.F. van Gunsteren, K. Allaart and P. Hofstra, Z. Phys. A 288 (1978) 49.
[5] H. Helppi et al., Nucl. Phys. A 357 (1981) 333.
[6] P.F. Mantica et al., Phys. Rev. C 42 (1990) 902.
[7] H. Dias and L. Losano, Phys. Rev. C 50 (1994) 1377.
[8] J. Toivanen and J. Suhonen, J. Phys. G 21 (1995) 1491.
[9] A. Holt, T. Engeland, E. Osnes, M. Hjorth-Jensen and J. Suhonen, Nucl. Phys. A 618 (1997) 107.
[10] M. Hjorth-Jensen, T.T.S. Kuo and E. Osnes, Phys. Rep. 261 (1995) 125.
[11] M. Waroquier and K. Heyde, Nucl. Phys. A 144 (1970) 481.
[12] K. Heyde and M. Waroquier, Nucl. Phys. A 167 (1971) 545.
[13] P. Ring and P. Schuck, The Nuclear Many-body Problem (Springer, Berlin, 1980).
[14] J. Suhonen, T. Taigel and A. Faessler, Nucl. Phys. A 486 (1988) 91.
[15] D.J. Rowe, Rev. Mod. Phys. 40 (1968) 153.
[16] C.A. Stone, J.D. Robertson, S.H. Faller, P.F. Mantica, B.E. Zimmerman, C. Chung and W.B. Walters, Phys. Scripta T 56 (1995) 316.
[17] H. Sagawa, O. Scholten, B.A. Brown and B.H. Wildenthal, Nucl. Phys. A 462 (1987) 1.
[18] A. Bohr and B.R. Mottelson, Nuclear Structure, Vol. I (Benjamin, New York, 1969).
[19] R. Machleidt, Adv. Nucl. Phys. 19 (1989) 189.
[20] R.R. Whitehead, A. Watt, B.J. Cole and I. Morrison, Adv. Nucl. Phys. 9 (1977).
[21] T. Engeland, M. Hjorth-Jensen, A. Holt and E. Osnes, Phys. Scripta T 56 (1995) 58.